GeoTerrace-2026-035

Spectral Characterization of Post-Fire Landscape Changes in Combat Zones Using Multitemporal Satellite Imagery

***A. Marchenko, I. Tsyhanenko-Dziubenko, T. Nazarenko, N. Ventsel**
(Zhytomyr Polytechnic State University)

SUMMARY

Combat-related landscape fires require spatially explicit assessment because active-fire detections, spectral burn severity, thermal anomalies, and vegetation recovery are represented at different spatial and temporal scales. This study develops an integrated geographic information system and remote sensing workflow for the Borodianka Territorial Community, Kyiv Oblast, using Sentinel-2 surface-reflectance imagery, Sentinel-3 land-surface-temperature products, and VIIRS active-fire detections, with meteorological and atmospheric reanalysis used as contextual evidence. The normalized burn ratio, differenced normalized burn ratio, and normalized difference vegetation index were calculated, and burn severity was interpreted using a four-class burned-area reflectance classification. VIIRS clusters identified the location and southwestward displacement of active burning, whereas Sentinel-2 raster analysis delimited a broader fire-affected envelope of 600-700 ha. Moderate to very high spectral damage occupied 280-370 ha, and mean vegetation greenness decreased by 35%. The strongest dNBR responses formed spatially coherent northern and central clusters that corresponded to the active-fire corridor. One year later, the share of critically altered NBR pixels had declined substantially, while higher NBR and NDVI classes expanded, indicating pronounced spectral recovery. The results demonstrate that multi-temporal spectral indices and GIS-based classification provide a reproducible framework for mapping fire extent, differentiating severity zones, and monitoring post-fire recovery where field access is constrained.

Keywords: Combat-related fires; Sentinel-2; VIIRS; NBR; dNBR; BARC; Burn severity; Vegetation recovery.

Corresponding Author: 25d_mas@liceum.ztu.edu.ua

Introduction

Landscape fires in active-conflict zones generate spatially heterogeneous surface changes that cannot be adequately represented by a single sensor or indicator. Fire-weather studies have shown that declining atmospheric humidity, rising temperature, and compound drought conditions increase wildfire potential (Jain et al., 2022; Richardson et al., 2022). These studies establish the meteorological context of fire activity but generally operate at regional to global scales and do not resolve the spatial structure of individual combat-related burn scars.

Remote sensing provides complementary observations of the fire process. VIIRS identifies active thermal anomalies at satellite overpass times (Schroeder et al., 2014), whereas Sentinel-2 supports detailed assessment of vegetation condition and burn severity through NBR, dNBR, and NDVI (Key & Benson, 2006). However, VIIRS detections are temporally discontinuous and cannot be interpreted as complete burn perimeters; dNBR and BARC thresholds remain sensitive to vegetation type, season, and local calibration; and the spatial resolutions of Sentinel-2, Sentinel-3, and atmospheric reanalysis are not directly commensurable. A methodological gap therefore remains in integrating active-fire observations, multi-temporal spectral-index rasters, and coarser contextual products within a single uncertainty-aware GIS workflow for conflict-affected territories with limited field access. The aim of this study is to assess the spatial extent, severity, and one-year recovery of combat-related landscape fires using Sentinel-2-derived NBR, dNBR, and NDVI, a four-class BARC interpretation, and VIIRS/FIRMS observations as independent spatial-temporal support.

Method and Theory

The geospatial database integrated Sentinel-2 Level-2A imagery (Copernicus Data Space Ecosystem, 2021) acquired on 18, 23, and 28 March and 7 April 2022 and 25 April 2023; Sentinel-3 SLSTR land-surface-temperature products for the same dates plus 29 March 2022; and VIIRS/FIRMS active-fire detections for 28-29 March. ECMWF meteorological fields and CAMS EAC4 carbon-monoxide data (Inness et al., 2019) were included only as regional contextual layers. Sentinel-2 clouds, shadows, defective pixels, and snow/ice classes were excluded using the Scene Classification Layer; the masked share remained below 6% for each scene. Band 12 was resampled from 20 to 10 m to establish a common analysis grid with Bands 4 and 8. Sentinel-3 retained its native 1 km information content and was compared with Sentinel-2 only at the level of generalized spatial patterns (Copernicus Sentinel Online, 2023). VIIRS detections were treated as overpass-time thermal observations rather than a continuous fire perimeter (Schroeder et al., 2014).

Raster calculations were performed in a projected GIS environment using NBR = (B8 - B12)/(B8 + B12), NDVI = (B8 - B4)/(B8 + B4), and dNBR = NBRpre - NBRpost. The 23 March and 7 April 2022 scenes represented the pre-fire and post-fire states. The dNBR raster was classified into four BARC-like severity classes: <0.10, 0.10-0.27, 0.27-0.44, and >0.44. For every date, class areas were calculated by raster zonal statistics and converted to hectares and percentages of the study polygon. Active-fire displacement was quantified from the shift of VIIRS cluster centroids relative to the downwind bearing. Spatial comparisons were restricted to scale-appropriate interpretation: 10 m Sentinel-2 products were analysed quantitatively, whereas 375 m VIIRS and 1 km Sentinel-3 products were used for event localization and contextual validation. All spatial layers were transformed to a common projected coordinate reference system before clipping, raster overlay, centroid analysis, and area calculation to minimize positional inconsistencies among datasets.

To improve comparability, all Sentinel-2 rasters were clipped to the same polygon, aligned to a 10 m grid, and checked for residual cloud, snow, and smoke effects. The analysis distinguishes three spatial products: (i) the instantaneous VIIRS active-burning footprint, (ii) the GIS-derived fire-affected envelope that includes areas between detections, and (iii) the Sentinel-2 burn-severity surface derived from dNBR and BARC classes. This separation prevents the active-fire footprint from being misreported as the final burned area and makes the uncertainty associated with sensor resolution explicit.

Results

VIIRS/FIRMS revealed several active-fire clusters on 28 March and a southwestward redistribution of detections by 29 March (Figure 1). Eight polygons represented an instantaneous active-burning footprint of 450-500 ha, while the GIS-derived fire-affected envelope, including intervening areas between detections, was estimated at 600-700 ha. The 2.5-3.0 km centroid displacement provided spatial-temporal evidence of fire progression. Its azimuth was consistent with the prevailing wind field, and the approximately 95% directional agreement supports this interpretation; however, the directional metric was treated as contextual validation rather than the central result of the spectral analysis.

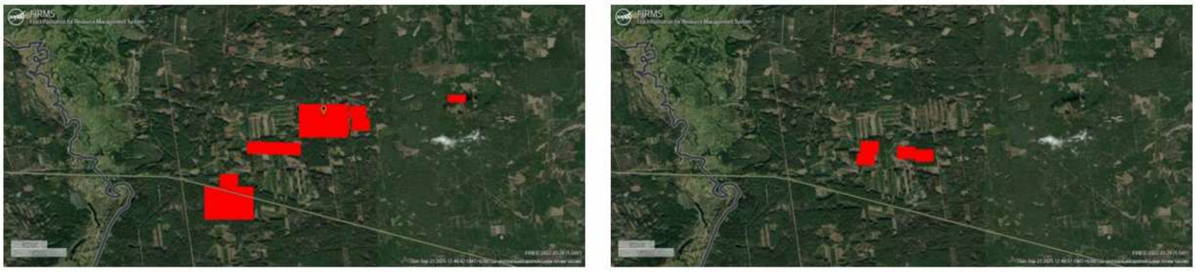

a) – VIIRS/FIRMS active-fire detections, 28 March 2022 *b) – VIIRS/FIRMS active-fire detections, 29 March 2022*

Figure 1. *Active-fire detections from VIIRS/FIRMS on: a - 28 March 2022; b - 29 March 2022*

The dNBR raster localized the strongest surface change in the northern and central clusters, while the four-class BARC interpretation converted the continuous change field into operational severity zones (Figure 2). Class 2 formed a broad transition belt of approximately 150-200 ha around the principal clusters. Class 3 occupied 100-120 ha in their cores, and class 4 was restricted to compact high-severity patches of 30-50 ha. Consequently, BARC classes 2-4 covered 280-370 ha. Their spatial arrangement, rather than the area of VIIRS polygons alone, provides the most defensible estimate of the severely affected surface. The concentric transition from compact high-dNBR cores to lower-severity margins also indicates a spatial gradient of vegetation and moisture loss rather than a uniform disturbance.

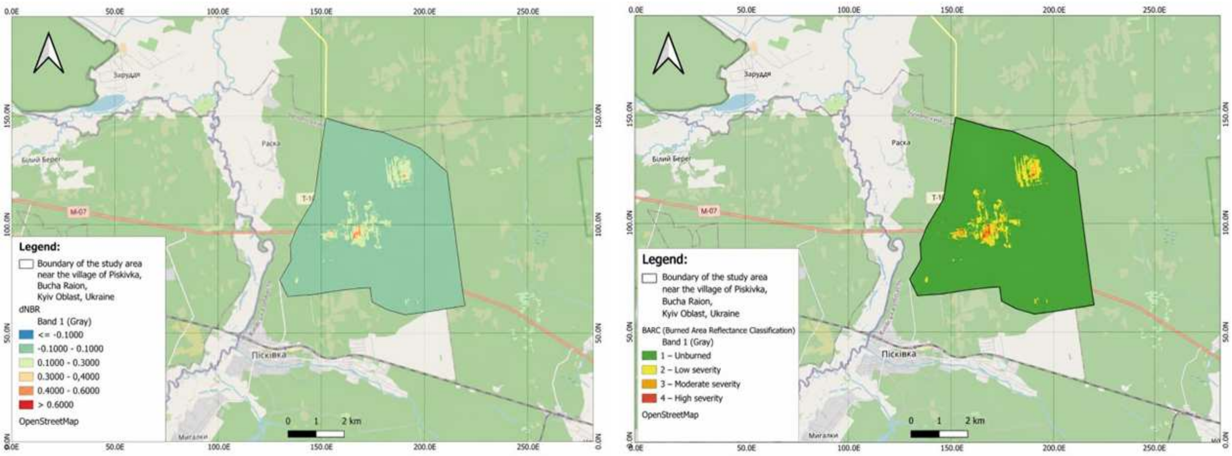

a) – dNBR map derived from Sentinel-2 imagery acquired on 23 March and 7 April 2022 *b) – Four-class BARC interpretation of burn severity*

Figure 2. *Spectral fire-severity mapping: a - dNBR from 23 March and 7 April 2022; b - four-class BARC interpretation*

Multi-temporal NBR analysis distinguished the pre-fire background, active disturbance, post-fire maximum, and recovery stage (Figure 3; Table 1). On 18-23 March, NBR values of 0.1-0.3

dominated 70-75% of the polygon. On 28 March, the first NBR <0 zones appeared over approximately 100 ha. By 7 April, the NBR ≤0 and 0-0.1 classes increased to 25% and 52%, respectively, so 77% of the area exhibited strong spectral alteration. By 25 April 2023, the NBR ≤0 class declined to 8%, while the 0.1-0.3 and 0.3-0.6 classes increased to 33% and 19%. Mean NDVI decreased from 0.31 to 0.20 (35%), but residual low-NDVI patches occupied less than 10% one year later. Agreement between NBR and NDVI supports vegetation recovery, although it does not prove restoration of pre-fire ecosystem structure or function.

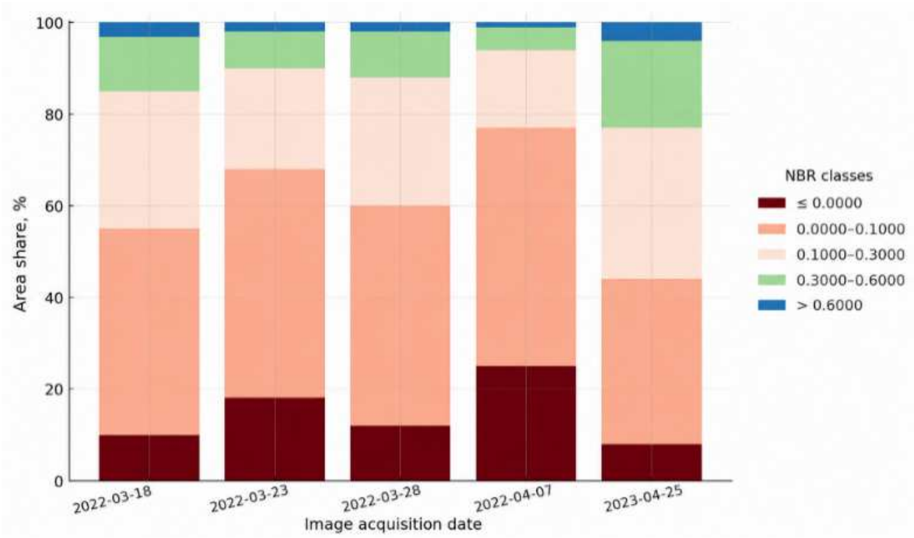

Figure 3. *Temporal distribution of the study area among NBR classes before, immediately after, and one year after the fire*

Table 1. *Multi-temporal spectral response of the study area*

Observation date	***Principal spectral response***	***Quantitative indicator***	***GIS/RS interpretation***
18-23 March 2022	NBR 0.1-0.3 dominated	70-75% of study area	Pre-fire early-spring baseline
28 March 2022	First NBR <0 clusters	Approximately 100 ha	Onset of detectable disturbance
7 April 2022	NBR ≤0 and 0-0.1 expanded	25% and 52%; 77% combined	Maximum mapped post-fire alteration
25 April 2023	Higher NBR classes expanded	NBR ≤0: 8%; 0.1-0.3: 33%; 0.3-0.6: 19%	Substantial spectral recovery

The combined indices provide complementary evidence: NBR traces temporal change, dNBR isolates the pre/post-fire difference, BARC converts that difference into severity classes, and NDVI independently records vegetation greenness. Their agreement reduces dependence on any single threshold.

Conclusions

The integrated GIS workflow enabled the differentiation of three fundamentally distinct spatial observations: instantaneous VIIRS active-fire detections, the broader GIS-derived fire-affected envelope, and the Sentinel-2-based spectral severity surface. This distinction is methodologically important because active-fire polygons represent thermal anomalies recorded at the time of satellite overpass and cannot be interpreted directly as the final extent of burned territory. The most consistent spatial relationship was observed between the VIIRS fire corridor and the principal northern and central clusters identified using dNBR and the four-class BARC interpretation. BARC classes 2-4 occupied approximately 280-370 ha, whereas the broader contextual fire-affected envelope covered 600-700 ha. Consequently, the BARC-derived area provides a more defensible estimate of spectrally confirmed fire severity than the complete GIS-defined envelope.

The combined analysis of NBR, dNBR, BARC, and NDVI demonstrated a coherent temporal transition from pre-fire conditions to maximum spectral disturbance and subsequent vegetation recovery. The proportion of the study area assigned to the NBR ≤ 0 class decreased from 25% immediately after the fire to 8% one year later, while low-NDVI patches contracted to less than 10% of the mapped territory. These changes indicate substantial post-fire revegetation during the first year of recovery. Nevertheless, the restoration of spectral-index values should not be interpreted as complete ecological recovery, because spectral greenness does not directly reflect the restoration of vegetation structure, species composition, or ecosystem functioning. Further research should incorporate field-based Composite Burn Index measurements, higher-resolution optical imagery, uncertainty analysis of classification thresholds, and object-based comparison of individual burn patches to transform the present screening workflow into a locally calibrated fire-severity assessment product.

References

Copernicus Data Space Ecosystem. (2021). Copernicus Sentinel-2 Collection 1 MSI Level-2A (L2A). https://sentinels.copernicus.eu/sentinel-data-access/sentinel-products/sentinel-2-data-products/collection-1-level-2a

Copernicus Sentinel Online. (2023). Copernicus Sentinel-3 SLSTR land user handbook (Issue 1.3). https://sentinels.copernicus.eu/documents/247904/4598082/Sentinel-3-SLSTR-Land-Handbook.pdf

Inness, A., Ades, M., Agustí-Panareda, A., Barré, J., Benedictow, A., Blechschmidt, A.-M., Dominguez, J. J., Engelen, R., Eskes, H., Flemming, J., Huijnen, V., Jones, L., Kipling, Z., Massart, S., Parrington, M., Peuch, V.-H., Razinger, M., Remy, S., Schulz, M., & Suttie, M. (2019). The CAMS reanalysis of atmospheric composition. Atmospheric Chemistry and Physics, 19, 3515-3556. https://doi.org/10.5194/acp-19-3515-2019

Jain, P., Castellanos-Acuna, D., Coogan, S. C. P., Abatzoglou, J. T., & Flannigan, M. D. (2022). Observed increases in extreme fire weather driven by atmospheric humidity and temperature. Nature Climate Change, 12, 63-70. https://doi.org/10.1038/s41558-021-01224-1

Key, C. H., & Benson, N. C. (2006). Landscape assessment. In FIREMON: Fire effects monitoring and inventory system (RMRS-GTR-164-CD, pp. LA-1-LA-55). U.S. Forest Service. https://research.fs.usda.gov/treesearch/24066

Richardson, D., Black, A. S., Irving, D., Matear, R. J., Monselesan, D. P., Risbey, J. S., Squire, D. T., & Tozer, C. R. (2022). Global increase in wildfire potential from compound fire weather and drought. npj Climate and Atmospheric Science, 5, 23. https://doi.org/10.1038/s41612-022-00248-4

Schroeder, W., Oliva, P., Giglio, L., & Csiszar, I. A. (2014). The new VIIRS 375 m active fire detection data product: Algorithm description and initial assessment. Remote Sensing of Environment, 143, 85-96. https://doi.org/10.1016/j.rse.2013.12.008